

Vibronic phenomena and exciton–vibrational interference in two-dimensional spectra of molecular aggregates

Vytautas Butkus and Leonas Valkunas

*Department of Theoretical Physics, Faculty of Physics,
Vilnius University, Sauletekio 9-III, 10222 Vilnius, Lithuania and
Center for Physical Sciences and Technology, Gostauto 9, 01108 Vilnius, Lithuania*

Darius Abramavicius*

*Department of Theoretical Physics, Faculty of Physics,
Vilnius University, Sauletekio 9-III, 10222 Vilnius, Lithuania and
State Key Laboratory of Supramolecular Complexes, Jilin University,
2699 Qianjin Street, Changchun 130012, PR China*

A general theory of electronic excitations in aggregates of molecules coupled to intramolecular vibrations and the harmonic environment is developed for simulation of the third-order nonlinear spectroscopy signals. The model is applied in studies of the time-resolved two-dimensional coherent spectra of four characteristic model systems: weakly / strongly vibronically coupled molecular dimers coupled to high / low frequency intramolecular vibrations. The results allow us to classify the typical spectroscopic features as well as to define the limiting cases, when the long-lived quantum coherences are present due to vibrational lifetime borrowing, when the complete exciton-vibronic mixing occurs and when separation of excitonic and vibrational coherences is proper.

I. INTRODUCTION

Excitonic energy spectrum of molecular aggregates experiences essential transformation due to the presence of high-frequency intramolecular vibrations. As a result, coupling between electronic excitations and intramolecular vibrations known as vibronic coupling turn to be responsible for a host of spectroscopically-observed phenomena. The vibronic effects have been investigated intensively by different theoretical methods since the foundation of molecular (Frenkel) exciton theory [1, 2]. Along with the advance of nonlinear spectroscopic techniques, some new insights related to coupling between electronic degrees of freedom of molecular aggregates and intramolecular vibrations were observed in third-order spectroscopic signals, for example, in two-dimensional (2D) coherent spectra demonstrating vibrational wave-packet motion, long-lived coherences, vibrational anisotropy beats, polaron formation, etc.[3–8]. Probably the most extensively discussed issue lately is the impact of discrete vibrational resonances on the electronic coherences and *vice versa*. These coherences are observed in the 2D electronic spectroscopy, but its possible role in energy transfer is currently under discussion [9–11].

Range and diversity of molecular systems, where vibronic coupling is very significant, appears to be extremely wide. Historically, molecular crystals were the first systems where the vibronic coupling was considered and the theoretical basis of the spectral characterization was developed by analyzing their stationary spectra [12–

15]. Further development of the theoretical approach was addressed to studies of vibronic excitations in H and J aggregates and in molecular films [16, 17]. Strong coupling to discrete intramolecular high-frequency modes of the C = C stretch vibration at around 1400 cm^{-1} together with the strong electrostatic interaction between the molecules are the most evident properties of the J-aggregates. Coupling to discrete low-frequency intramolecular modes (160 cm^{-1} , for example[18, 19]) has also been considered. Significant vibronic features are prevalent in spectra of aggregated and strongly-coupled molecular dimeric dyes, the formation of which is usually the first step towards the large-scale molecular aggregation [20–25].

Photosynthetic pigment–protein (P–P) complexes could be considered as yet another class of molecular systems, where weak vibronic coupling (however, only recently observed) was found to be important [10, 26–30]. Since pigment molecules within P–P formations are weakly-coupled and the surrounding protein framework is ready to dissipate any vibrational motion of the pigments, the domination of electronic coupling over vibronic effects is commonly assumed. Therefore, long-lasting oscillations in coherent 2D spectra were initially explained by purely excitonic coherences [31–33]. Recently, vibronic components and mixing of both, electronic and vibronic, ingredients have been reported [34, 35].

If we were to represent the above-mentioned systems as points on a schematic two-dimensional phase space, where the axes indicate vibrational frequency and electronic resonance interaction, the most of it would be covered as presented in Fig. 1. We can make a classification of the points scattered over the plot by considering the possible time-resolved experiment with ultra-short laser pulses of typical bandwidth of $\sim 1000 - 2000$

*Electronic address: darius.abramavicius@ff.vu.lt

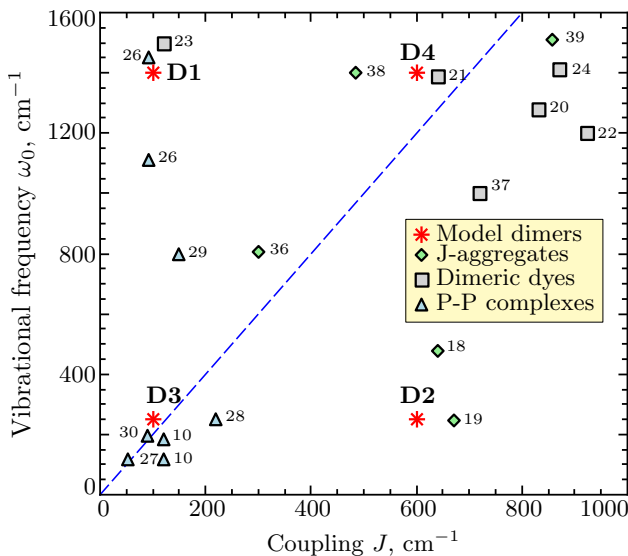


Fig. 1: Experimentally and theoretically investigated molecular systems (dimeric dyes, weakly-coupled P-P complexes, J-aggregates and films), characterized by different electronic resonance interactions J and vibrational frequencies ω_0 . Dashed line indicates the region of exciton-vibronic resonance ($\omega_0 = 2J$), the numbers next to symbols are the references to the corresponding studies. Stars indicate the model dimer systems considered in this paper.

cm^{-1} . In the top-left corner of the figure we then have the weakly-coupled systems with high-frequency vibrations. In this case the experiment would resolve a few peaks of the vibronic progression at most and the splittings due to electronic coupling would be overlapping. The mixed case where electronic resonance interactions and vibronic progression would be resolvable along with strong quantum-mechanical mixing of both types of transitions, is present in the top-right part of the scheme. The laser spectrum would cover only a few peaks in this case. On the bottom-left corner we have the mixed systems again, but the laser pulse spectrum could cover all peaks. And, finally, on the bottom-right corner we have the case where the full vibrational progression could be observed in the experiment and the electronic splitting would be well-resolved.

To cover all these cases in an unified model, we present the molecular exciton-vibronic theory developed for the purpose of its application in describing the two-dimensional electronic spectroscopy signals. It is based on the Holstein-type exciton-vibronic Hamiltonian with assumption of multi-particle vibronic state basis [12, 40]. Dissipation is included by coupling the vibrational coordinate to the harmonic bath. Special attention is paid to exciton-vibronic resonances, at which the most pronounced mixing of states is present [35, 41–43]. Four different models of dimer systems are chosen for consideration as indicated by stars in Fig. 1: two being considerably away from the exciton-vibronic resonance (**D1** and **D2**) and another two corresponding to mixed con-

ditions (**D3** and **D4**). As one can observe, these models represent four typical molecular systems: weakly-coupled P-P complexes with high and low-frequency vibrations (**D1** and **D3**), the J-aggregate (**D2**) and a molecular dye (**D4**). Therefore, the conclusions drawn from the results of model systems are general in terms of its application to different molecular aggregates.

II. VIBRATIONAL AGGREGATE MODEL

Various models of a molecule coupled to continuum of bath vibrations were developed within the framework of the perturbative system-bath interaction expansion[44]. The bath is then described by the spectral density function, which represents auto-correlations of the electronic *site* energy fluctuations due to the environment. The most popular model assumes the Brownian particle-like vibrational motion of the molecule in a solvent [45, 46]. This model is usually enough to obtain proper spectral lineshapes in simulations of systems with no expressed high-frequency vibrations at fixed temperature. For systems with well-resolved high-frequency modes of vibrations the spectral density approach is applied by including a δ -shaped or finite-bandwidth peak into the bath spectral density function. The δ -peak does give everlasting coherent beats in the coherent 2D spectra[47, 48], while in case of finite-width peak decay of oscillations is obtained due to pure dephasing [49, 50]. However, this method has two deficiencies. Firstly, it neglects the effects caused by quantum-mechanical mixing of the vibronic levels of different molecules when the vibronic splitting is comparable to the intermolecular excitonic coupling. Secondly, it does not include vibrational relaxation as the vibrations are assumed to be in thermal equilibrium at fixed temperature. These could be important effects when the coupling to vibrations is strong.

There have been several studies of nonlinear coherent spectra of molecular dimers with exciton-vibronic mixing included [35, 42, 51]. However, the realistic molecular aggregates contain several dozens or hundreds of molecules. We develop a general description applicable for molecular aggregates with an arbitrary number of chromophores.

Let us start with the displaced oscillator model of a molecule. It dictates that the Hamiltonian of a single (say m -th) molecule in an aggregate can be given by

$$\hat{H}_m = \left[\frac{\hat{p}_m^2}{2} + \frac{\omega_m^2}{2} \hat{q}_m^2 \right] |g^m\rangle\langle g^m| + \left[\epsilon_m + \frac{\hat{p}_m^2}{2} + \frac{\omega_m^2}{2} (\hat{q}_m - d_m)^2 \right] |e^m\rangle\langle e^m|. \quad (1)$$

Here \hat{p}_m and \hat{q}_m are the momentum and coordinate operators of the intramolecular vibrational motion, ω_m is the vibrational frequency and d_m is the displacement in the excited state. The effective mass of the oscillator is taken as unity. Ground and excited state wavevectors for the m -th molecule, $|g^m\rangle$ and $|e^m\rangle$ (we use superscript

indices for later convenience) respectively, in the space of electronic states of the single molecule comprise the complete basis set, thus $|g^m\rangle\langle g^m| + |e^m\rangle\langle e^m| = 1$. After introducing operators for electronic excitations \hat{B}_m^\dagger , so that $|e^m\rangle = \hat{B}_m^\dagger|g^m\rangle$, and its Hermitian conjugate \hat{B}_m , we can write

$$\hat{H}_m = \frac{\hat{p}_m^2}{2} + \frac{\omega_m^2}{2}\hat{q}_m^2 + (\epsilon_m + \lambda_m - \omega_m^2 d_m \hat{q}_m) \hat{B}_m^\dagger \hat{B}_m. \quad (2)$$

Here we defined the reorganization energy $\lambda_m = \omega_m^2 d_m^2 / 2$. As the molecule can be electronically excited just once, we must have $\hat{B}_m^\dagger |e^m\rangle = 0$ or $\hat{B}_m \hat{B}_m^\dagger + \hat{B}_m^\dagger \hat{B}_m = 1$, which reflects the fermionic property.

By inserting the bosonic creation and annihilation operators for the vibrational degrees of freedom

$$\hat{p}_m = i\sqrt{\frac{\omega_m}{2}} (\hat{b}_m^\dagger - \hat{b}_m) \quad \text{and} \quad \hat{q}_m = \sqrt{\frac{1}{2\omega_m}} (\hat{b}_m^\dagger + \hat{b}_m)$$

into Eq. (2), one gets the fully quantized Hamiltonian of the m -th molecule,

$$\hat{H}_m = \omega_m \left(\hat{b}_m^\dagger \hat{b}_m + \frac{1}{2} \right) + [\epsilon_m + \lambda_m - \omega_m \sqrt{s_m} (\hat{b}_m^\dagger + \hat{b}_m)] \hat{B}_m^\dagger \hat{B}_m. \quad (3)$$

Here the Huang–Rhys factor is defined as $s_m \equiv \lambda_m / \omega_m$. This brings the vibrational ladder of states in the electronic ground state

$$|g_i^m\rangle = \frac{(\hat{b}_m^\dagger)^i}{\sqrt{i!}} |0\rangle \quad (4)$$

and in the electronic excited state

$$|e_i^m\rangle \equiv \hat{B}_m^\dagger |g_i^m\rangle = \hat{B}_m^\dagger \frac{(\hat{b}_m^\dagger)^i}{\sqrt{i!}} |0\rangle. \quad (5)$$

$|0\rangle$ is the vacuum state in terms of electronic and vibrational excitations.

A. Hamiltonian of the vibrational aggregate

The Hamiltonian of an aggregate of realistic molecules involves three components: electronic states, vibrational structure for each electronic state and the Coulomb coupling between all electronic and vibronic levels. The first two are described by extending the Hamiltonian of a single molecule into the space of a set of molecules within the Heitler–London approximation, which assumes that the aggregate states are constructed from the direct products of the molecular single excitations [1, 45, 46, 52]. We consider only single and double excitations. The Coulomb coupling between the m -th and n -th molecule is denoted

by the resonant electronic coupling constant J_{mn} and the corresponding term is as follows:

$$\hat{H}_{\text{Coulomb}} = \sum_{m \neq n} J_{mn} \hat{B}_m^\dagger \hat{B}_n. \quad (6)$$

We neglect electrostatic interactions between vibrations in the ground state. Within this model the Hamiltonian for the vibrational aggregate is given by

$$\hat{H} = \sum_m \left[\epsilon_m + \lambda_m - \omega_m \sqrt{s_m} (\hat{b}_m^\dagger + \hat{b}_m) \right] \hat{B}_m^\dagger \hat{B}_m + \sum_m \omega_m \left(\hat{b}_m^\dagger \hat{b}_m + \frac{1}{2} \right) + \sum_{m \neq n} J_{mn} \hat{B}_m^\dagger \hat{B}_n. \quad (7)$$

Similarly as to the electronic aggregate we get bands corresponding to electronic states, but now the ground state $|g\rangle$ of the aggregate is not a single quantum level, but a band of vibrational states. Thus, there are states with all chromophores in their electronic ground states, while vibrational excitations are arbitrary:

$$|g_{(i_1 i_2 \dots i_N)}\rangle \equiv \left| \prod_m g_{i_m}^m \right\rangle = \left[\prod_m \frac{(\hat{b}_m^\dagger)^{i_m}}{\sqrt{i_m!}} \right] |0\rangle. \quad (8)$$

Here i_m is a quantum number of vibrational excitation of the m -th molecule. Thus $|g_{i_m}^m\rangle$ now denotes the electronic ground state of the m -th molecule being in the i_m -th vibrational level.

The singly-excited states are obtained by assuming that one of the molecules is in its electronic excited state, while the others are in their arbitrary vibrational ground states. We thus get the set of states

$$|e_{n,(i_1 i_2 \dots i_N)}\rangle \equiv |e_{i_n}^n \prod_{\substack{m \\ m \neq n}} g_{i_m}^m \rangle = \hat{B}_n^\dagger \left[\prod_m \frac{(\hat{b}_m^\dagger)^{i_m}}{\sqrt{i_m!}} \right] |0\rangle. \quad (9)$$

The doubly-excited states are obtained similarly,

$$|f_{kl,(i_1 i_2 \dots i_N)}\rangle \equiv |e_{i_k}^k e_{i_l}^l \prod_{\substack{m \\ m \neq k,l}} g_{i_m}^m \rangle = \hat{B}_k^\dagger \hat{B}_l^\dagger \left[\prod_m \frac{(\hat{b}_m^\dagger)^{i_m}}{\sqrt{i_m!}} \right] |0\rangle. \quad (10)$$

State ordering $k < l$ is satisfied here. A complete basis set is included into the model since all possible combinations (multi-particle states) of vibronic and vibrational excitations are considered, cf. single-particle approximation, where only states $|e_{i_n}^n \prod_{\substack{m \\ m \neq n}} g_0^m \rangle$ are included [13, 53]. The index notation is further simplified by introducing the N -component vector $\mathbf{i} = (i_1 i_2 \dots i_N)$. Then the basis states can be written as $|g_{\mathbf{i}}\rangle$, $|e_{n,\mathbf{i}}\rangle$ and $|f_{kl,\mathbf{i}}\rangle$.

In this setup electronic and vibrational subsystems are coupled only through term $(\hat{b}_m^\dagger + \hat{b}_m) \hat{B}_m^\dagger \hat{B}_m$ in Hamiltonian (Eq. (7)). It thus induces the shifts of electronic

energies by creation or annihilation of vibrational quantum. Otherwise, electronic and vibrational subsystems are independent. The basis set is chosen accordingly. The other basis set is possible by using shifted vibrational excitations in the electronic excited states [41, 54]. However, our approach gives convenient form for various matrix elements and allows us to easily incorporate the environment as shown below. Hamiltonian of the ground state manifold in this basis is diagonal,

$$H_{i,j}^{(\text{gg})} = \left[\sum_m \omega_m \left(i_m + \frac{1}{2} \right) \right] \delta_{ij}, \quad (11)$$

where $\delta_{ij} \equiv \prod_m \delta_{i_m j_m}$. Similarly, the Hamiltonian of singly-excited states is given by

$$\begin{aligned} H_{i,j}^{(\text{e}_n \text{e}_k)} &= \delta_{nk} \left[\epsilon_n + \lambda_n + \sum_m \omega_m \left(i_m + \frac{1}{2} \right) \right] \delta_{ij} \\ &\quad - \delta_{nk} \omega_n \sqrt{s_n} \langle i_n, j_n \rangle \prod_{\substack{m \\ m \neq n}} \delta_{i_m j_m} \\ &\quad + (1 - \delta_{nk}) J_{nk} \delta_{ij}, \end{aligned} \quad (12)$$

where we have defined the vibrational wavefunction overlap $\langle i_n, j_n \rangle = \sqrt{i_n} \delta_{i_n, j_n+1} + \sqrt{j_n} \delta_{i_n, j_n-1}$. For the double-exciton states we have

$$\begin{aligned} H_{i,j}^{(\text{f}_{kl} \text{f}_{k'l'})} &= \\ &\delta_{kk'} \delta_{ll'} \left[\epsilon_k + \epsilon_l + \lambda_k + \lambda_l + \sum_m \omega_m \left(i_m + \frac{1}{2} \right) \right] \delta_{ij} \\ &\quad - \delta_{kk'} \delta_{ll'} \omega_k \sqrt{s_k} \langle i_k, j_k \rangle \prod_{\substack{m \\ m \neq k}} \delta_{i_m j_m} \\ &\quad + \delta_{kk'} \delta_{ll'} \omega_l \sqrt{s_l} \langle i_l, j_l \rangle \prod_{\substack{m \\ m \neq l}} \delta_{i_m j_m} \\ &\quad + [\delta_{kk'} (1 - \delta_{ll'}) J_{ll'} + \delta_{ll'} (1 - \delta_{kk'}) J_{kk'}] \delta_{ij}. \end{aligned} \quad (13)$$

The exciton energies (eigenstate basis) ϵ_e and ϵ_f are obtained by numerically diagonalizing matrices defined above. The bands of singly- and doubly-excited states are however much more complicated than those of the electronic aggregate due to coupling between the singly-excited vibronic subbands. In the eigenstate basis all these substates become mixed. The unitary transformation to the eigenstate basis is thus as follows:

$$|e_p\rangle = \sum_n \sum_i \psi_{p,i}^n |e_{n,i}\rangle, \quad (14)$$

$$|f_r\rangle = \sum_{\substack{kl \\ k < l}} \sum_i \Psi_{r,i}^{kl} |f_{kl,i}\rangle. \quad (15)$$

Note that for high vibronic numbers i, j the Franck-Condon parameter becomes small and these states do not contribute to the spectra. In general, if one includes ν vibrational levels in description of each of N molecules, this results in $N\nu^N$ singly-excited states, and $N(N-1)\nu^N/2$

doubly-excited states, enumerated by indices p and r in the previous expressions, respectively.

For electronic excitations we consider the dipole operator defined as

$$\hat{\mathbf{P}} = \sum_m^N \mathbf{d}_m (\hat{B}_m^\dagger + \hat{B}_m), \quad (16)$$

where \mathbf{d}_m is the electronic transition dipole vector of the m -th molecule. This form essentially reflects the Frank-Condon approximation where the electronic transition is not coupled to vibrational system. The dipole moments representing transitions from the ground state to singly-excited states and from singly-excited state to the doubly-excited states are given by

$$\boldsymbol{\mu}_{g_i}^{e_p} = \langle g_i | \hat{\mathbf{P}} | e_p \rangle = \sum_m^N \mathbf{d}_m \psi_{p,i}^m$$

and

$$\boldsymbol{\mu}_{e_p}^{f_r} = \langle e_p | \hat{\mathbf{P}} | f_r \rangle = \sum_{m,n}^N \sum_i \mathbf{d}_k \psi_{p,i}^n \Psi_{r,i}^{(mn)}.$$

The transition amplitudes thus have the mixed electronic-vibronic nature encoded in eigenvectors $\psi_{p,i}^n$ and $\Psi_{r,i}^{(mn)}$.

B. Coupling to the bath

We next include the relaxation using a microscopic dephasing theory, based on the linear coupling of the vibronic coordinate to the harmonic overdamped bath [55]. Hence, we assume that the vibronic coordinate is damped. The bath is described as a set $\{\alpha\}$ of harmonic oscillators, whose Hamiltonian is:

$$\hat{H}_B = \sum_\alpha \frac{1}{2} \hat{p}_\alpha^2 + \frac{1}{2} \omega_\alpha^2 \hat{x}_\alpha^2. \quad (17)$$

Here \hat{p}_α is the momentum and \hat{x}_α is the coordinate operators and ω_α is the frequency of the α -th bath oscillator. The system-bath interaction is then given in the bilinear form

$$\hat{H}_{\text{SB}} = \sum_{m\alpha} z_{m\alpha} \hat{x}_\alpha \hat{q}_m = \sum_{m\alpha} \sqrt{\frac{z_{m\alpha}^2}{2\omega_m}} \hat{x}_\alpha (\hat{b}_m^\dagger + \hat{b}_m). \quad (18)$$

We add these two operators to complete the Hamiltonian in Eq. (7). Thus, the off-diagonal fluctuations of vibronic levels translate into diagonal fluctuations of the electronic-only aggregates due to electronic excitation creation/annihilation operators in Eq. (18). More explicitly, coupling z induces the vibronic off-diagonal

couplings and causes vibrational intramolecular relaxation. Resonance intermolecular interaction J will extend into the electronic energy relaxation between different molecules. The non-zero fluctuating matrix elements in the site basis (Eqs. (8)–(10)) are very simple:

$$\left(\hat{H}_{\text{SB}}\right)_{i,j}^{(\text{gg})} = \langle g_i | \hat{H}_{\text{SB}} | g_j \rangle = \mathcal{H}(i, j), \quad (19)$$

$$\left(\hat{H}_{\text{SB}}\right)_{i,j}^{(e_n e_k)} = \langle e_{n,i} | \hat{H}_{\text{SB}} | e_{k,j} \rangle = \delta_{nk} \mathcal{H}(i, j), \quad (20)$$

$$\left(\hat{H}_{\text{SB}}\right)_{i,j}^{(f_{kl} f_{k'l'})} = \langle f_{kl,i} | \hat{H}_{\text{SB}} | f_{k'l',j} \rangle = \delta_{kk'} \delta_{ll'} \mathcal{H}(i, j). \quad (21)$$

Here we defined an auxiliary function of bath-space fluctuations

$$\mathcal{H}(i, j) = \sum_{m\alpha} \sqrt{\frac{z_{m\alpha}^2}{2\omega_m}} \langle i_m, j_m \rangle \hat{x}_\alpha \prod_{s \neq m} \delta_{i_s j_s}. \quad (22)$$

Notice, that interband fluctuations are absent, so the interband relaxation (electronic relaxation to the ground state) is not included. Transformation to the eigenstate basis yields the fluctuations of the eigenstate characteristics. In the ground state manifold we have eigenstates equivalent to the site basis since the corresponding Hamiltonian is diagonal (Eq. (11)). For the manifold of singly-excited states we get

$$\left(\hat{H}_{\text{SB}}\right)_{p_1 p_2}^{(\text{ee})} = \sum_m \sum_{i,j} \psi_{p_1,i}^{m*} \psi_{p_2,j}^m \mathcal{H}(i, j), \quad (23)$$

and for the manifold of doubly-excited states

$$\left(\hat{H}_{\text{SB}}\right)_{r_1 r_2}^{(\text{ff})} = \sum_{\substack{m,n \\ m>n}}^N \sum_{i,j} \Psi_{r_1,i}^{(mn)*} \Psi_{r_2,j}^{(m_1 n_1)} \mathcal{H}(i, j). \quad (24)$$

The quantities of interest, which describe the relaxation properties, are the correlation functions of fluctuating Hamiltonian elements. Firstly, we assume that fluctuations of different chromophores are independent. Therefore, we can sort out and associate the bath coordinates to specific molecules. Since the bath oscillators are independent, correlation functions of the operator in the Heisenberg representation with respect to the thermal equilibrium are uncorrelated, $\langle \hat{x}_\alpha(t) \hat{x}_\beta(0) \rangle = \delta_{\alpha\beta} \langle \hat{x}_\alpha(t) \hat{x}_\alpha(0) \rangle$, and we can obtain separated baths of different molecules. Secondly, we assume that the different molecules have statistically the same surroundings, so the system–bath coupling is fully characterized by the following single fluctuation correlation function:

$$C_0(t) = \sum_{m\alpha} \frac{z_{m\alpha}^2}{2\omega_m} \langle \hat{x}_\alpha(t) \hat{x}_\alpha(0) \rangle. \quad (25)$$

For the infinite number of bath oscillators they can be conveniently expressed using the spectral density $\mathcal{C}''(\omega)$

[44]:

$$C_0(t) = \frac{1}{\pi} \int_{-\infty}^{+\infty} \frac{1}{1 - e^{-\beta\omega}} e^{-i\omega t} \mathcal{C}''(\omega) d\omega, \quad (26)$$

where $\beta = (k_B T)^{-1}$ is the inverse thermal energy. Using these functions we get the eigenstate fluctuation correlation functions $C_{ab,cd}(t) = \langle \left(\hat{H}_{\text{SB}}(t)\right)_{ab} \left(\hat{H}_{\text{SB}}\right)_{cd} \rangle = C_0(t) h_{ab,cd}$ for different manifolds. For the electronic ground state manifold where a single eigenstate is equivalent to the original basis state $|g_i\rangle$ it yields

$$C_{ij,kl}^{(\text{gg})}(t) = C_0(t) \sum_m \langle i_m, j_m \rangle \langle k_m, l_m \rangle \prod_{s \neq m} \delta_{i_s j_s} \delta_{k_s l_s}. \quad (27)$$

We use the shorthand vector notations $\mathbf{i}_s^- = (i_1, i_2, \dots, i_{s-1}, i_s - 1, i_{s+1}, \dots, i_N)$ and $\mathbf{i}_s^+ = (i_1, i_2, \dots, i_{s-1}, i_s + 1, i_{s+1}, \dots, i_N)$, which allow us to explicitly write:

$$C_{ij,kl}^{(\text{gg})}(t) = C_0(t) \sum_s \left\{ \sqrt{i_s j_s} \delta_{i_s^+} \delta_{k_l^+} + \sqrt{(i_s + 1) j_s} \delta_{i_s^-} \delta_{k_l^+} + \sqrt{i_s (k_s + 1)} \delta_{i_j^+} \delta_{k_s^+ l} + \sqrt{(i_s + 1) (k_s + 1)} \delta_{i_s^-} \delta_{k_s^+ l} \right\}. \quad (28)$$

Similarly, one can obtain the correlation functions involving the singly- and doubly-excited states $C_{p_1 p_2, p_3 p_4}^{(\text{ee})}(t)$, $C_{p_1 p_2, r_1 r_2}^{(\text{ef})}(t)$ and $C_{r_1 r_2, r_3 r_4}^{(\text{ff})}(t)$ (see Appendix A for the corresponding expressions).

C. Population transfer

As the bath induces off-diagonal fluctuations in all three bands of states one has to consider the population transfer inside the excited and ground manifolds (the populations of the doubly-excited states are never created so the transport is not relevant there). The propagator $G_{e_{p_2} e_{p_1}}(t_2)$ denotes the conditional probability of the excitation to be transferred to state $|e_{p_2}\rangle \langle e_{p_2}|$ from $|e_{p_1}\rangle \langle e_{p_1}|$ in time t_2 . Similarly, $G_{g_j g_i}(t_2)$ is the propagator in the electronic ground manifold. In this model the bath is considered as the intermolecular modes which should be Markovian while intramolecular vibrational coordinates are considered explicitly. Hence, the Redfield theory applies for the Markovian bath. Within the secular Redfield theory [45], both types of propagators satisfy the Pauli master equation,

$$\frac{\partial}{\partial t} G_{ab}(t) = \sum_{c \neq a} k_{a \leftarrow c} G_{cb}(t) - \sum_{c \neq a} k_{c \leftarrow a} G_{ab}(t). \quad (29)$$

Here indices a , b and c can be either excited state numbers, or vectors, indicating vibrational ground states.

$k_{a \leftarrow c}$ are the transfer rates in the excited (further on denoted by $k_{e_{p_2} \leftarrow e_{p_1}}$) or ground state ($k_{g_j \leftarrow g_i}$). Using the Redfield relaxation theory, one can obtain simple expressions for the rates

$$k_{e_{p_2} \leftarrow e_{p_1}} = h_{e_{p_2} e_{p_1}, e_{p_1} e_{p_2}} C'''(\omega_{e_{p_1} e_{p_2}}) \left[\coth\left(\frac{\beta \omega_{e_{p_1} e_{p_2}}}{2}\right) + 1 \right] \quad (30)$$

for the excited state population transfer. For the ground state vibrational relaxation, one has only two subsets of nonzero terms,

$$k_{g_{i_s}^- \leftarrow g_i} = i_s C'''(\omega_s) \left[\coth\left(\frac{\beta \omega_s}{2}\right) + 1 \right] \quad (31)$$

and

$$k_{g_{i_s}^+ \leftarrow g_i} = (i_s + 1) C'''(-\omega_s) \left[\coth\left(-\frac{\beta \omega_s}{2}\right) + 1 \right]. \quad (32)$$

With these transformation expressions now it is possible to develop the general theory describing the spectroscopic properties of vibronic aggregates.

III. RESULTS

In the theory of the vibronic aggregate described above we derived all identities necessary to simulate the third-order signals in the frame of the second-order cumulant expansion of the system response function [44]. The system response function of an electronic-only aggregate is defined as a sum of contributions (or so-called Liouville space pathways) responsible for *bleaching* of the ground state (B), photon-induced (stimulated) *emission* from the excited state (E) and *induced absorption* of a photon in the excited state (A). They are conveniently represented by the double-sided Feynman diagrams, which show the system evolution during the delay times t_1 , t_2 and t_3 between the interactions. In diagrams, ground- or excited-state populations or coherences evolve during delay time t_2 (Fig. 2a). Additionally, since population state can be transferred during t_2 in the excited state, the so-called population transfer pathways \tilde{S}_E and \tilde{S}_A are added up (Fig. 2b). In the case of vibronic aggregate, this formalism has to be extended to take into account multi-level ground state. Therefore, additional diagrams with coherences and population transfer in the ground-state manifold have to be included. This ingredient and the resulting final expressions for the two-dimensional coherent spectra is described in Appendix B.

To discuss the outcomes of the developed system response function theory for the molecular aggregate, we consider a molecular dimer (MD) as the simplest molecular complex exhibiting vibronic phenomena, as well as the exciton-vibrational interference. The vibrational frequencies, site energies and Huang-Rhys factors of the constituent molecules are taken to be the same and are

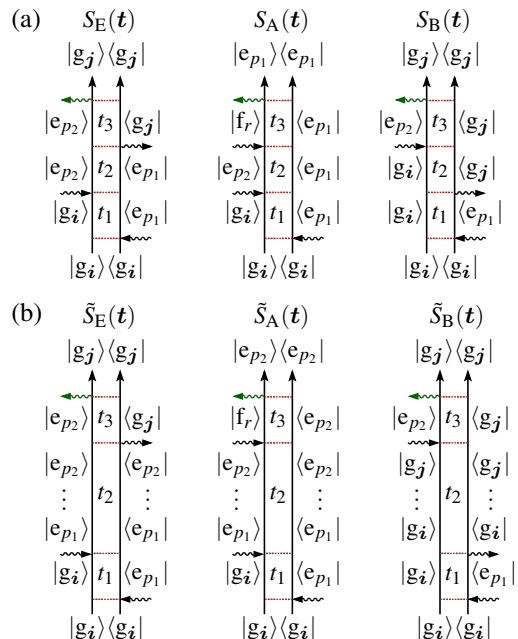


Fig. 2: System response function of the rephasing signal of the vibronic aggregate is represented by 6 double-sided Feynman diagrams without population transfer (a) and with population transfer (b). The diagrams are denoted as responsible for stimulated emission (E), excited state absorption (A) and ground-state bleaching (B) processes.

denoted by $\omega_0 \equiv \omega_1 = \omega_2$, $\epsilon \equiv \epsilon_1 = \epsilon_2 = 1200 \text{ cm}^{-1}$ and $s = s_1 = s_2$, respectively. Also, we analyze the models in the case of weak system-bath coupling (with Huang-Rhys factor equal to $s = 0.05$) and strong coupling ($s = 0.5$). Four distinct parameter sets are used and we denote the corresponding models as **D1-D4**, indicated by stars in Fig. (1).

In the **D1** model the resonant coupling constant is taken to be $J = 100 \text{ cm}^{-1}$ and the vibrational frequency is chosen to be $\omega_0 = 1400 \text{ cm}^{-1}$. Such parameters are typical for the photosynthetic pigment-protein complexes, for example, the photosynthetic antenna of cryptophyte protein phycoerythrin 545 (the Huang-Rhys factor is 0.1) [26]. We denote this model as the weakly-coupled P-P complex with high-frequency vibration.

In the **D2** model resonant coupling of $J = 600 \text{ cm}^{-1}$ and vibrational frequency $\omega_0 = 250 \text{ cm}^{-1}$ is used. These numbers are typical parameters of J-aggregates, coupled to low-frequency intramolecular vibrations. For example, in 2D electronic spectra of PVA/C8O3 tubular J-aggregates, oscillations associated to the 160 cm^{-1} vibration is observed and the strongest coupling between the molecules is in a range of $640\text{--}1110 \text{ cm}^{-1}$ as it was shown by Milota *et al.* [18]. In the same study, the experimental Fourier maps were obtained. In J-aggregates the coupling to vibrations for individual chromophores is known to decrease due to exciton delocalization [53]. It means that, if the aggregate is approximated as a dimer, the Huang-Rhys factor of the monomer should be mul-

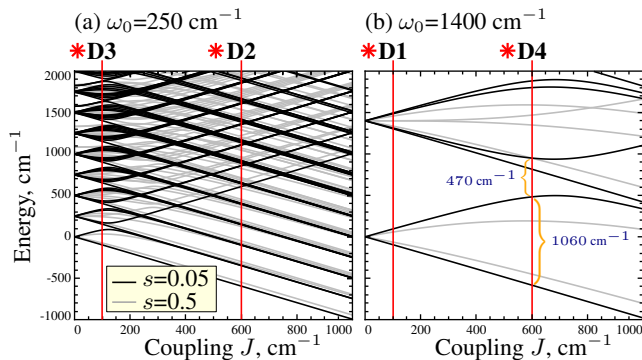


Fig. 3: Dependencies of the singly-excited state energies on the electronic resonance interaction (J coupling) in the case of the vibrational frequency $\omega_0 = 250 \text{ cm}^{-1}$ (a) and 1400 cm^{-1} (b). The Huang–Rhys factor is $s = 0.05$ (black lines) and $s = 0.5$ (gray lines). Resonant coupling constants corresponding to models **D1**–**D4** are indicated by the red vertical lines.

multiplied by factor of $N/2$ where N is a number of chromophores in the aggregate in the case of complete state delocalization. Therefore, a very strong coupling to vibrations should be considered. In our case, **D2** model with $s = 0.5$ represents the typical J-aggregate better.

Parameters of the **D3** model ($J = 100 \text{ cm}^{-1}$, $\omega_0 = 250 \text{ cm}^{-1}$) are, as in the **D1** model, typical for the P-P complexes. In such molecular systems strong coupling to discrete low-frequency vibrations are present. For example, in the measurements of two-color photon echo of the light-harvesting complex phycocyanin-645 from cryptophyte marine algae, long-lived oscillations possibly associated to the 194 cm^{-1} vibrational mode were observed [30]. Similar parameters were also considered to be relevant for the Fenna–Mathews–Olsen (FMO) photosynthetic light-harvesting complex [42]. Therefore, we assume that the **D3** model effectively represents the weakly-coupled P-P complex coupled to a low-frequency vibrational mode.

Presence of strong resonance electronic interaction between molecules and strong coupling with high-frequency vibrations is typical for many dimeric dyes. Hence, in the **D4** model, the main parameters are set to $J = 600 \text{ cm}^{-1}$ and $\omega_0 = 1400 \text{ cm}^{-1}$ to be similar to ones of perylene bisimide dye with the Huang–Rhys factor of 0.6 [56].

The bath, whose degrees of freedom are not treated explicitly, is represented by the Debye spectral density $C''(\omega) = 2\lambda\omega/(\omega^2 + \gamma^2)$ which represents the low-frequency fluctuations. In order to get the similar homogeneous broadening in all cases of Huang–Rhys factors, the value of $\lambda s = 25 \text{ cm}^{-1}$ is kept constant throughout all simulations. The solvent damping energy is set to $\gamma = 50 \text{ cm}^{-1}$. The molecular transition dipole vectors are taken to have unitary lengths and their orientations are spread by an angle $\alpha = 2\pi/5$. Temperature is set to 150 K ($\beta^{-1} \approx 104 \text{ cm}^{-1}$).

Let us consider the manifold of singly-excited states of all **D1**–**D4** models. It consists of superpositions of elec-

tronic singly-excited states and vibrational excitations of the constituent molecules. The energy dependence on the resonant coupling constant reveals a complex composition of the states within the singly-excited state manifold (Fig. 3). For uncoupled molecules ($J = 0$) the ladder-type pattern of vibrational energy states is present as the energies are equally separated by ω_0 . Increasing coupling produces the excitonic splitting which can be seen as the red shift of the lowest energy state and appearance of two ladder-type progressions. However, the interaction of vibronic and electronic states induces repulsion of the energy levels, which is mostly evident where the ladders experience crossing, i.e. in the vicinity of the so-called avoided crossing regions [41]. We denote the corresponding parameters for which the crossings occur as the exciton–vibronic resonances. The complete mixing of the electronic and vibronic substates is obtained for these resonances. The energy level repulsion effect is more pronounced in the case of $s = 0.5$ (see the gray lines in Fig. 3).

In models **D1** and **D2** the vibrational frequency ω_0 and resonant coupling constant J differs significantly and we are reasonably away from the resonance as can be seen in Figures 1 and 3 (the corresponding resonant coupling values are indicated by vertical lines in the later one). Therefore, these models can be considered as rather pure systems of vibrational and electronic aggregates, respectively. On the contrary, parameters of the **D3** and **D4** models assure that the system is very close to the exciton–vibronic resonances and the spectroscopic signals will be more complex due to mixing.

Properties of the model dimers are reflected in linear absorption spectra (Fig. 4). The **D1** system has intermolecular coupling of the same order as the absorption linewidth. Hence, both electronic transitions (and excitonic splitting) become hidden inside the single peak 12000 cm^{-1} when the Huang–Rhys factor is $s = 0.05$. Another peak at $\sim 13500 \text{ cm}^{-1}$ comes from the one-quantum level of the vibrational progression and becomes stronger for $s = 0.5$ (red dashed line).

The **D2** model is completely opposite to the **D1**. The excitonic splitting is large and two absorption peaks approximately at 11500 cm^{-1} and 12700 cm^{-1} show the excitonic system character. As the vibrational frequency is small, we find the vibrational progression on both excitonic lines dependent on the Huang–Rhys factor. The **D1** and **D2** systems, more or less, behave "additively" where the excitonic contributions and the vibrational progressions add up in absorption.

Models **D3** and **D4** are very different. In the **D3**, both parameters, the excitonic resonance interaction and the vibrational frequency, are small and the absorption spectrum shows a single broad line at $\sim 12000 \text{ cm}^{-1}$. While excitonic and vibrational contributions are mixed, as shown in Fig. 3a, surprisingly, the absorption spectrum is relatively simple with a single electronic peak shaped by the vibrational progression. However the shape is strongly dependent on the Huang–Rhys factor:

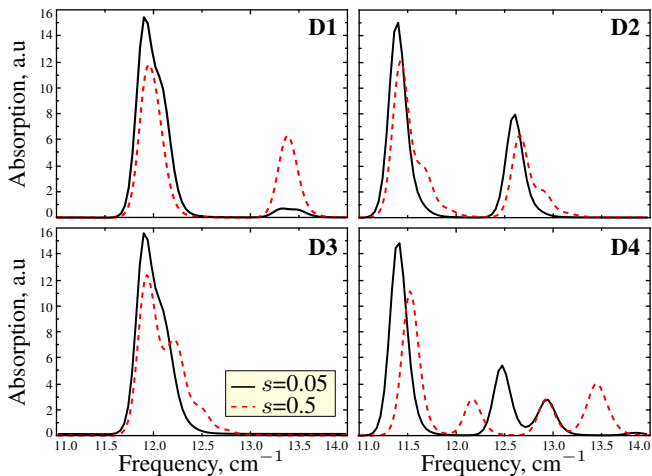


Fig. 4: Absorption spectra of dimers **D1–D4** in case of Huang–Rhys factors $s = 0.05$ (black solid line) and $s = 0.5$ (red dashed line).

for $s = 0.05$, one can guess two excitonic bands (black solid line), while for $s = 0.5$, the excitonic spectrum disappears and the vibrational progression is observed.

The fine features of mixed system is better seen in the model **D4**, which has large energy splittings between levels compared to the **D3**. The **D4** model shows non-trivial spectrum even for small value of the HR factor. There is a single lower-excitonic peak at 11500 cm^{-1} , but the higher-excitonic peak is split into two ($\sim 12500 \text{ cm}^{-1}$ and $\sim 13000 \text{ cm}^{-1}$). The large HR factor makes the spectrum even more complicated where we find four peaks and they all are due to superpositions of vibrational and electronic nature. Hence both **D3** and **D4** systems reflect the mixed *vibronic* features of the molecular dimer.

The two-dimensional electronic spectroscopy has been suggested as being able to distinguish between the origin of transitions of such systems. So we analyze transition types, which could be resolved by means of this spectroscopy for our models **D1–D4**. The 2D spectra reveal as a set of peaks – all of them contain oscillatory contributions in the population delay time. The so-called Fourier maps are useful for the analysis of the origin of the oscillations in 2D spectra [18, 33, 50, 57–60]. Thus, the maps are calculated by fitting the evolution of each point of the 2D spectrum by the exponentially decaying function and performing the Fourier transform of the residuals over the delay interval t_2 ,

$$A(|\omega_1|, \omega_2, \omega_3) = \int_0^{\infty} e^{-i\omega_2 t_2} S_{\text{residuals}}(|\omega_1|, t_2, \omega_3) dt_2. \quad (33)$$

The amplitude and phase which completely describe the oscillations of every point of the 2D spectrum are then extracted from the complex function $A(|\omega_1|, \omega_2, \omega_3)$. As the dependence of the amplitude on frequency ω_2 oscillation is available for every point of ω_1 and ω_3 , we suggest first to introduce a representative variable that would

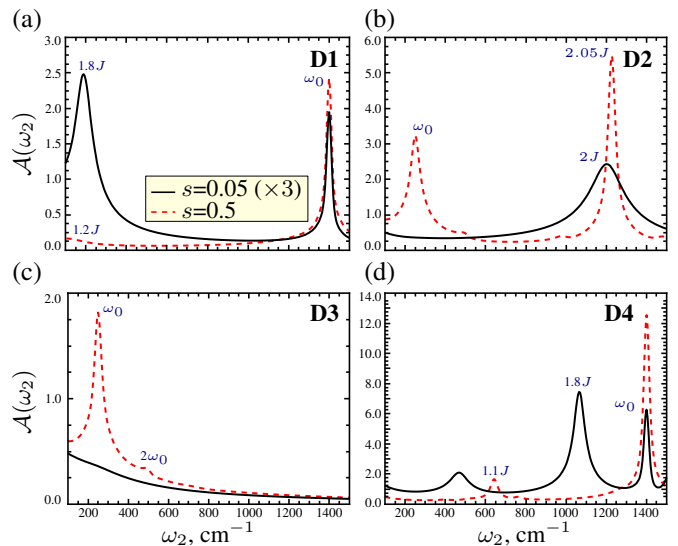


Fig. 5: Maximum of the Fourier amplitudes characterizing oscillations in the 2D spectra of the model dimers **D1–D4** (a–d panels, respectively) in case of Huang–Rhys factors $s = 0.05$ (black solid lines) and $s = 0.5$ (red dashed lines). The frequency values of the peaks are indicated in the graph.

characterize which oscillation frequencies are important, in general. The maximum of the Fourier amplitude as a function of ω_2 can be used for that:

$$\mathcal{A}(\omega_2) = \max [|\text{Abs } A(|\omega_1|, \omega_2, \omega_3)|]_{\omega_2 = \text{const.}}$$

The $\mathcal{A}(\omega_2)$ dependencies on the oscillation frequency for the **D1–D4** models are depicted in Fig. 5 and the Fourier maps of several dominant frequencies are presented in Figures 6 and 7. We next discuss the models separately.

A. **D1** model. Weakly-coupled P-P complex with high-frequency vibration

Two dominant frequencies of 190 cm^{-1} and 1400 cm^{-1} representing oscillations in spectra of the **D1** system are resolved when $s = 0.05$ (Fig. 5a). Hence we consider Fourier maps at these two frequencies. The former corresponds to the excitonic energy splitting, but the frequency is smaller than $2J$ ($190 \text{ cm}^{-1} \approx 1.8J$) due to slight energy level repulsion, present even away from the exciton–vibronic resonance. The map for $\omega_2 = 190 \text{ cm}^{-1}$ is typical for electronic coherence, as the oscillating behavior corresponding to the excited state absorption and ground state bleaching contributions are positioned symmetrically with respect to the diagonal and the oscillations are in-phase (Fig. 6a). Since the distance between the positions is smaller than the homogeneous linewidth, the most intensive oscillations are present on the diagonal due to constructive interference. The Fourier map at $\omega_2 = 1400 \text{ cm}^{-1}$ is a typical reflection of the vibrational/vibronic coherence as the oscillations are present

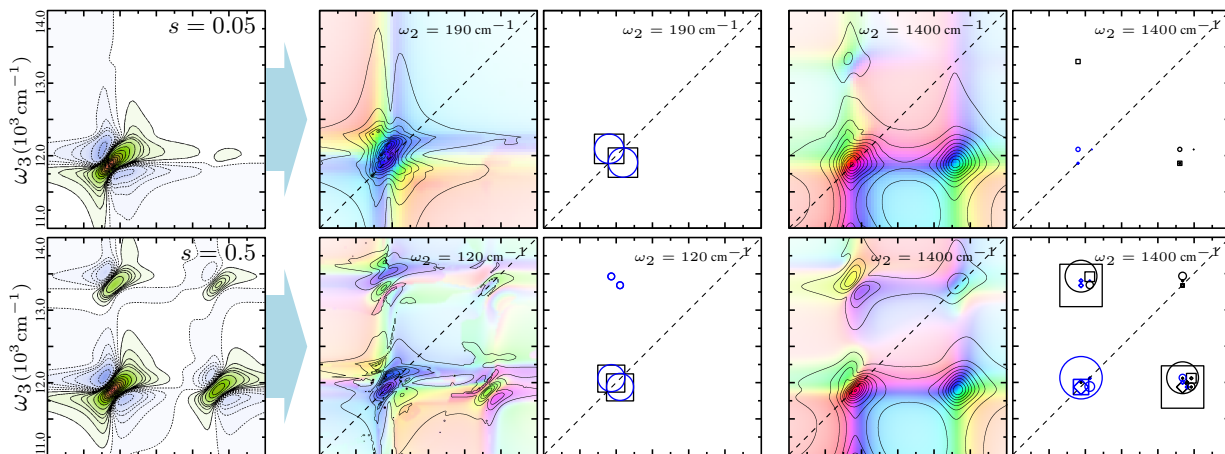
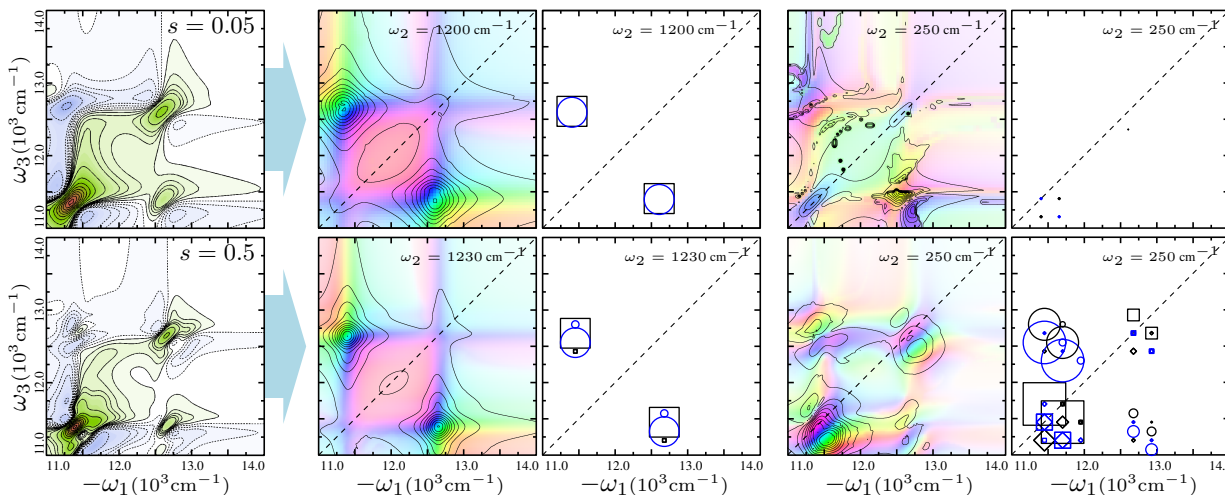
(a) **D1 model. Weakly-coupled P-P complex with high-frequency vibration**(b) **D2 model. J-aggregate**

Fig. 6: Oscillations in 2D spectra of weakly-coupled P-P complex with high-frequency vibration (**D1** model) and J-aggregate (**D2** model) in case of weak and strong coupling to vibrations ($s = 0.05$ and $s = 0.5$, respectively). 2D rephasing spectra at $t_2 = 0$ and two most significant Fourier maps are represented in rows of every model with. Schemes of the oscillations-providing contributions (\circ – excited state absorption, \square – stimulated emission and \diamond – ground state bleaching) are presented next to the maps. The size of the symbols are proportional to the amplitude of the corresponding contribution.

both on the diagonal line and on the cross-peaks, characterized by complex phase dependence [43]. The phase of oscillations is shifted by π at the center of the lower diagonal peak compared to the centers of the other peaks, which is also typical for beatings of vibrational/vibronic coherences [57]. Two more off-diagonal oscillating features at around $\omega_3 = 10500 \text{ cm}^{-1}$ are out of bounds in presented Fourier maps, hence they would be off-resonant in a typical experiment.

Increasing the Huang–Rhys factor to $s = 0.5$ causes stronger mixing in the system. The shape of the Fourier map at $\omega_2 = \omega_0$ does not change notably, however, its amplitude increases by factor of 3. The Fourier map at $\omega_2 = 120 \text{ cm}^{-1} \approx 1.2J$ closely resembles the map at $\omega_2 = 190 \text{ cm}^{-1}$ when $s = 0.05$. Additional contributions of the excited state absorption appear above the diagonal. Features in this map are not very smooth since the

lifetime of oscillations is much shorter (note that symbol sizes in Fig. 5a, representing the amplitudes of contributions in the schemes for $s = 0.05$ and $s = 0.5$ are, however, similar).

B. D2 model. J-aggregate.

The strongest frequencies for model **D2** are 250 cm^{-1} and 1250 cm^{-1} (Fig. 5b). The Fourier map of the **D2** system at $\omega_2 = \omega_0 = 250 \text{ cm}^{-1}$ clearly shows the large contribution from the ground state and excited state vibrations on the diagonal and less significant excited state absorption features in the cross-peaks (Fig. 6b). The oscillations are more intensive below the diagonal, which is consistent with the maps of the above-mentioned PVA/C8O3 J-aggregate[18]. If compared, the

relative intensities of oscillations associated with electronic ($\omega_2 \approx 2J$) and vibrational ($\omega_2 \approx \omega_0$) transition, one would find that the relative intensity of electronic coherences has a tendency to decrease when increasing the Huang–Rhys factor. Thus, for $s \gg 1$, maps would be completely dominated by the vibrational coherences. The maps at $\omega_2 = 1200 \text{ cm}^{-1}$ and $\omega_2 = 1230 \text{ cm}^{-1}$ in Fig. 6b are typical for electronic coherences as the oscillations are diagonal-symmetric. Note that the energy splitting is much larger than the homogeneous linewidth and the two peaks in the maps are distinguished, cf. to the corresponding Fourier maps in the **D1** model.

C. D3 model. Weakly-coupled P-P complex with low-frequency vibration

Assignment of oscillations in the **D3** with strongest peaks shown in Fig. 5c is complicated since the parameters are close to the exciton-vibronic resonance (Fig. 3a). It might appear that there is only a continuum of low-frequency oscillations in the spectra for $s = 0.05$ since the maximum amplitude dependence on the frequency does not contain any peaks (Fig. 5c). However, there are short-lived oscillations at $\omega_2 = 180 \text{ cm}^{-1}$ and $\omega_2 = 250 \text{ cm}^{-1}$, but their Fourier maps are not distinguishable (Fig. 7a). Increasing the Huang–Rhys factor to $s = 0.5$ enhances the $\omega_2 = \omega_0$ oscillation which, as it can be seen in the scheme next to the map in Fig. 7a, is a mixture of many different contributions.

D. D4 model. Strongly-coupled dimeric dye

The absorption spectrum of the **D4** model changes drastically when increasing the Huang–Rhys factor (Fig. 4). Both transition frequencies and intensities are redistributed due to sensitivity of the energy spectrum at the avoided crossing region. In the 2D spectra for $s = 0.05$, there are 3 clearly separable long-lived oscillations of frequencies $\omega_2 = 0.8J \approx 470 \text{ cm}^{-1}$, $\omega_2 = 1.1J \approx 1060 \text{ cm}^{-1}$ and $\omega_2 = \omega_0$ (Fig. 5d). The later two correspond to the excitonic energy splitting and vibrational coherence, respectively, while the 470 cm^{-1} oscillation signifies beatings between the lower and upper states in the avoided crossing region (the corresponding energy level gaps are indicated in Fig. 3b). For $s = 0.5$ the level repulsion effect is even more pronounced, as the gap between the lowest energy states decreases from $1.8J$ to $1.1J$ and the gap of the avoided crossing region increases from $0.8J$ to $1.3J$.

The Fourier maps allow us to separate electronic and vibrational coherences in this particular mixed case. When $s = 0.05$ (Fig. 7b) the Fourier map for $\omega_2 = 1060 \text{ cm}^{-1}$ is typical for electronic coherence. The only signature of coupling to vibrations is the oscillatory contribution of the excited state absorption appearing above the stimulated emission. It indicates that doubly-excited

state manifold is effectively shifted up due to vibronic coupling and, therefore, the peaks are elongated along ω_3 axis in the Fourier maps. The $\omega_2 = 1400 \text{ cm}^{-1}$ map is exceptionally created by the ground state vibrations, however, the energy level structure in the excited state manifold is reflected as the distance between some oscillating features in the Fourier maps are found to be equal to 1060 cm^{-1} (see the labels with arrows in Fig. 7b).

The $\omega_2 = 1400 \text{ cm}^{-1}$ oscillation becomes mixed if $s = 0.5$. As it can be seen in the corresponding scheme of oscillations, contributions from all types of diagrams appear and heavily congest the Fourier map. The lowest diagonal peak becomes oscillating due to stimulated emission and ground state bleaching contributions. The map for the $\omega_2 = 640 \text{ cm}^{-1}$ oscillation is similar to one for $\omega_2 = 1060 \text{ cm}^{-1}$ presented above. Stronger coupling to vibrations induce appearance of additional oscillations in the excited state manifold, seen as two peaks above the diagonal.

IV. DISCUSSION

2D electronic spectroscopy is the ultimate tool capable to directly reflect coherent system dynamics, manifested by spectral oscillations and beatings. Frequency and decay rate of oscillations indicate the energy difference of states involved in the coherent superposition and the coherent state lifetime, respectively. Positions of emerging oscillations in spectra are conveniently depicted by the use of Fourier maps, thus providing us one more additional dimension. For example, peaks in the maps, symmetric with respect to the diagonal, reflect the electronic coherence evolution in the excited state (**D1** and **D2** models in Fig. 6). The information about the phase of oscillations provides additional information about the ongoing processes. Therefore, fitting the experimental data by means of the simulated Fourier maps would lead to unambiguous conclusions.

A. Nature of coherences

Let us discuss about the quantum coherences in molecular aggregates. Quantum mechanical description of *electronic* excitation treats the rigid constituent molecule’s skeleton as the potential energy surface for electrons. The resulting electron density dynamics after photoexcitation can be approximated by the oscillatory electric dipole moment. Thus, the coupling between the molecules produces the discrete energy levels in the single excited manifold of the *electronic* aggregate. In a similar way, if intramolecular vibrations are considered in an isolated molecule, the harmonic/anharmonic oscillator model for the electronic ground and excited states can be applied. This also results in discrete spectrum of *vibrational* levels. These two pictures merge due to the intermolecular coupling and the electronic and vi-

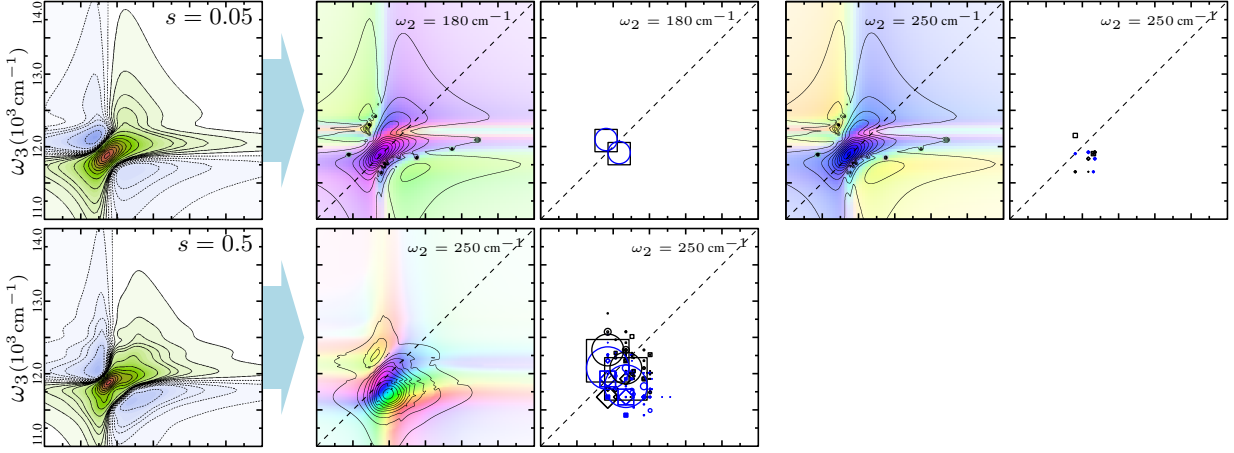
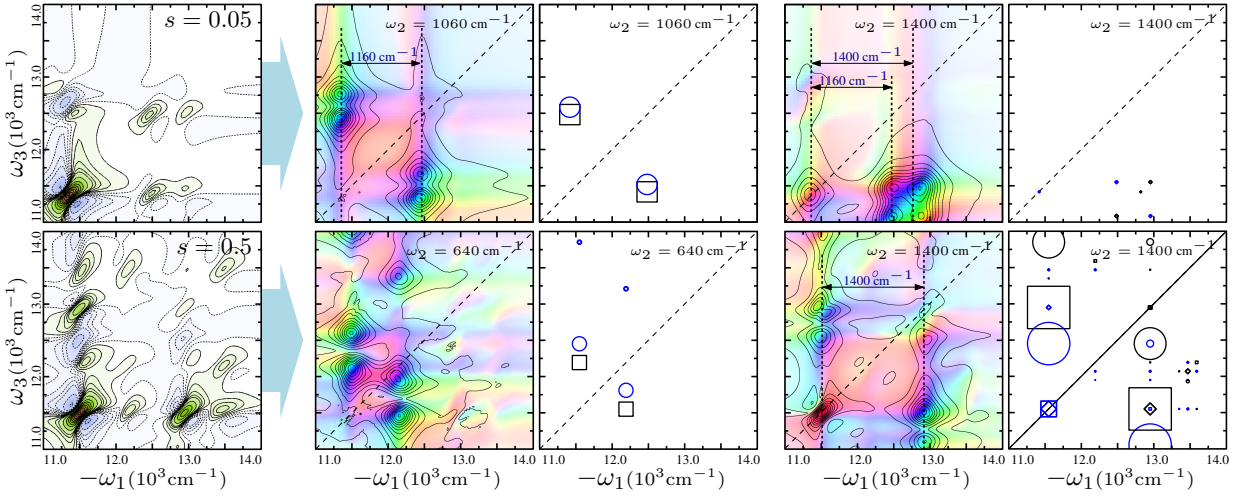
(a) **D3 model. Weakly-coupled P-P complex with low-frequency vibration**(b) **D4 model. Strongly-coupled dimeric dye**

Fig. 7: Oscillations of a weakly-coupled P-P complex with low-frequency vibration (**D3** model) and strongly-coupled dimeric dye (**D4** model). Presentation is analogous to Fig. 6.

brational subsystems mix up. It is then natural to try to quantify, how much of electronic or vibrational character is inherited in the composite system. However, this often leads to many ambiguities, for example, in linear spectra of J-aggregates[39].

There have been many attempts to unambiguously distinguish between vibrational, vibronic and excitonic coherences visible as oscillations in 2D spectra. However, the question of how to do that is proper only if mixing in the system is low. As it was shown here, two conditions for low mixing can be distinguished: (i) the coupling between vibrational and electronic subsystem has to be weak (small Huang–Rhys factor); (ii) the system must not be in a vicinity of exciton–vibronic resonance, represented by the avoided crossing region in the energy spectrum. These conditions are best met for high-frequency intramolecular vibrations in weakly-coupled P–P complexes and low-frequency vibrations in strongly-coupled aggregates, the **D1** and **D2** models, respectively.

In the case of substantial mixing of the coherences

of electronic and vibrational character, the information about the transition composition can be evaluated from coherent oscillations in some cases. It is most obvious in the **D2** model representing the case of the J-aggregate, when the electronic system is strongly coupled to low-frequency vibration (second row in Fig. 6b). Despite the strong mixing the Fourier map for the electronic frequency ($\omega_2 = 1230 \text{ cm}^{-1}$) contains diagonal-symmetric features, similar to those present in the weak mixing case. In the **D4** model, which stands as an equivalent of the strongly-coupled dimeric dye, the mixture of coherences for $\omega_2 = 1060 \text{ cm}^{-1}$ and $\omega_2 = 1400 \text{ cm}^{-1}$ can also be disentangled ($s = 0.05$, Fig. 7b). Firstly, the Fourier map at $\omega_2 = 1060 \text{ cm}^{-1}$ contains diagonal-symmetric peaks, which would suggest, that this particular coherence is rather electronic. Secondly, there are features in the map at $\omega_2 = 1400 \text{ cm}^{-1}$ separated by 1400 cm^{-1} and 1060 cm^{-1} as well as the peak on the diagonal exhibiting high-frequency oscillations. The latter fact as well as the obviously stronger oscillations below the diagonal shows

that the origin of the 1400 cm^{-1} oscillation is rather vibrational. The similar analysis can be applied to the **D4** model with $s = 0.5$, where the mere evidence of vibrational content is the diagonal oscillating peak in the $\omega_2 = 1400\text{ cm}^{-1}$ map.

One cannot discriminate between coherences of dominating electronic or vibrational character in weakly-interacting photosynthetic complexes, coupled to low-frequency vibrations. This is clearly demonstrated by the **D3** model in both cases of weak and strong electron-phonon coupling (first and second rows in Fig. 7, respectively). The coherences in the system are highly mixed and no typical patterns, which were present in the Fourier maps of the other systems, are found here. The Fourier map in case of strong coupling to vibrations is composed of many contributions, evolving in the ground and excited states (the second row in Fig. 7), thus, indicating complete state character mixing. Hence, the *electronic* or *vibrational* transitions are properly qualified, while *vibronic* and *how-much-vibronic* is a vague concept and should be avoided. Instead one should treat such coherences as simply mixed, which is completely a proper concept in quantum mechanics.

B. Lifetime of coherences in aggregates

The fact that some coherences are less visible in the Fourier maps is to high degree related to their lifetimes. Obviously, oscillations which decay fast will be vaguely captured by the Fourier transform or even will not be present in the maps at all. Let us now concentrate on the maximum of the Fourier amplitude dependence on frequency, $\mathcal{A}(\omega_2)$, in case of $s = 0.05$, presented by the solid lines in Fig. 5. The widths of the peaks are given by the lifetime of the corresponding oscillations.

The lifetime of the vibrational ground state coherence depends only on the overlap of vibrational frequency and bath spectral density. It can be deduced from Eqs. (31) and (32). For example, the lifetime of $|g_0g_0\rangle\langle g_0g_1|$ coherence $\tau_{01} = 2(\gamma_{g_0g_0} + \gamma_{g_0g_1})^{-1}$ is ~ 3 ps for $\omega_0 = 1400\text{ cm}^{-1}$ and the width of the corresponding peak in the $\mathcal{A}(\omega_2)$ dependence is $\sim 40\text{ cm}^{-1}$ (Fig. 5a and d). The lifetime of $\omega_0 = 250\text{ cm}^{-1}$ coherence is ~ 500 fs, thus, the corresponding peak in $\mathcal{A}(\omega_2)$ is very broad and, therefore, hardly distinguishable (Fig. 5b and c). This effect essentially depends on the spectral density function (including the shape and the amplitude) and its value at the corresponding vibrational frequency [61].

The lifetimes of coherences in the excited state manifold are not that trivial. On one hand, transfer rates relating electronic states of purely electronic aggregates depend on the absolute value of the bath spectral density at the corresponding frequency. Additionally, they depend on extend of delocalization of a particular state. On the other hand, transfer rates between vibronic states of a single molecule are the same as of the ground state vibrational states. In our case, these two pictures are

merged and the lifetimes of mixed coherences cannot be expressed in simple terms.

It has been shown, that the lifetimes of vibronic coherences increase significantly, if the electronic transitions are close to vibrational frequencies even if the Huang-Rhys factor is small ($s < 0.1$) [10, 42]. This is evident in the $\mathcal{A}(\omega_2)$ dependencies, as well: the lifetime of the $\omega_2 = 1.8J$ oscillation in the **D1** model is smaller than the corresponding lifetime of the frequency oscillation in the **D4** model by factor of ~ 1.8 while the lifetimes of the $\omega_2 = \omega_0$ coherences are identical. If compared, $\omega_2 = 2J$ oscillations in the **D2** model decay at least 3 times faster than the $\omega_2 = 1.8J$ oscillations in the **D4** model.

If the Huang-Rhys factors are large ($s \gtrsim 0.5$), low-frequency vibrational coherences in the ground state decay faster than in the case of weak coupling to vibrations discussed above (see dashed lines in Fig. 5). This is due to the lower value of the reorganization energy, which is $\lambda = 50\text{ cm}^{-1}$ for $s = 0.5$ (cf. $\lambda = 500\text{ cm}^{-1}$ for $s = 0.05$). Stronger interaction with vibrations induces more mixing in the system. Therefore, we can see long-lived coherences of $\omega_2 = 2.05J$ in the **D2** model. We can thus conclude that the electronic coherences effectively borrow some lifetime from the vibrational coherences due to the quantum mechanical mixing. The mixing and borrowing of the dipole strength in excitonic systems is a well-known phenomenon, however the lifetime borrowing is poorly discussed.

C. Energetic disorder

Energetic disorder is yet another important parameter for the coherent state evolution. It was shown for molecular dimer with vibrations, that in the case of substantial energy disorder, coherences of prevailing vibrational/vibronic character will dominate over those of rather electronic character [43]. From the discussion above it follows that this effect will be more significant for rather pure systems: weakly-coupled P-P complexes with high-frequency vibrations and J-aggregates (**D1** and **D2** models, respectively). In both cases vibrational coherences will dominate in the Fourier maps, while the electronic coherences will dephase fast because of combined influence of the energetic disorder and the lifetime of the state. In the mixed systems (**D3** and **D4**) the result will be more complicated. The reason behind is that the mixing occurs when resonances match, i.e. at the exciton-vibronic resonance. Disorder will make the matching less significant for most of ensemble members show less mixing. Hence, the electronic and vibronic character for a disordered ensemble is better defined and should be better identified in experiments.

V. CONCLUSIONS

In this paper, theory of molecular aggregate with intramolecular vibrations for coherent spectroscopy was presented. It accounts for incoherent and coherent effects caused by excitonic coupling and exciton–vibronic interaction. The molecular dimer model is used for simulation purposes of typical systems in a wide range of parameters to reflect pigment–protein complexes, J-aggregates or dimeric molecular dyes.

Regarding the question of distinguishing the electronic, vibronic or vibrational coherences, we conclude that the question itself is fully defined and proper only if the character of states is pure (electronic or vibrational). We have shown that such a separation is indeed possible for systems, where the resonant coupling and vibrational frequency is off-resonant, i.e. the system is away from the so-called exciton–vibronic resonance. The analysis of oscillations in mixed systems is of qualitative significance and allows us to tell if the specified oscillation is of the mixed origin. The frequencies of transitions, involved in the mixture can be resolved.

The positions of oscillating features must be taken into careful consideration when analyzing experimental data. There are spectral regions of mixed systems, where oscillations exceptionally due to coherences in the ground or excited states can be found, thus providing more information about system composition. For example, the property that features in the Fourier maps are asymmetric with respect to the diagonal is the signature that the corresponding state is mixed.

Lifetime of excitonic coherences is mostly determined by the coupling to discrete modes of intramolecular vibrations. These modes, on their own, are coupled to the continuum of low-frequency bath fluctuations, represented by the spectral density. Thus, the overlap of the spectral density function and frequencies of intramolecular vibrations as well as the form of spectral density function directly influences the lifetime of electronic coherences.

Appendix A: Correlation functions involving singly- and doubly-excited states

Singly-excited eigenstates are obtained by unitary transformation, and we get the same symmetry properties as for

$$C_{p_1 p_2, p_3 p_4}^{(ee)}(t) = C_0(t) \sum_{m,n} \sum_{i,j} \sum_{\mathbf{k},\mathbf{l}} \sum_a \psi_{p_1,i}^{m*} \psi_{p_2,j}^m \psi_{p_3,\mathbf{k}}^{n*} \psi_{p_4,\mathbf{l}}^n \times \langle i_a, j_a \rangle \langle k_a, l_a \rangle \prod_{\substack{s \\ s \neq a}} \delta_{i_s j_s} \delta_{k_s l_s}. \quad (\text{A1})$$

Here the first sum is over different chromophores, the second and third sum is over the vibrational levels of the whole aggregate and finally the sum over a is over the different vibrational modes (which is identical to the number of sites since each site has one vibrational coordinate). We then get the following result:

$$C_{p_1 p_2, p_3 p_4}^{(ee)}(t) = C_0(t) \sum_{i,\mathbf{k}} \sum_s \left\{ \sqrt{i_s k_s} \xi_{i_s^-}^{(p_1 p_2)} \xi_{\mathbf{k}_s^-}^{(p_3 p_4)} + \sqrt{(i_s + 1) k_s} \xi_{i_s^+}^{(p_1 p_2)} \xi_{\mathbf{k}_s^-}^{(p_3 p_4)} + \sqrt{i_s (k_s + 1)} \xi_{i_s^-}^{(p_1 p_2)} \xi_{\mathbf{k}_s^+}^{(p_3 p_4)} + \sqrt{(i_s + 1)(k_s + 1)} \xi_{i_s^+}^{(p_1 p_2)} \xi_{\mathbf{k}_s^+}^{(p_3 p_4)} \right\}.$$

Here

$$\xi_{i_s^\pm}^{(p_a p_b)} = \sum_n \psi_{p_a, i}^{n*} \psi_{p_b, i_s^\pm}^n. \quad (\text{A2})$$

For the functions involving the double excitations we can write similarly

$$C_{p_1 p_2, r_1 r_2}^{(ef)}(t) = C_0(t) \sum_{i,\mathbf{k}} \sum_s \left\{ \sqrt{i_s k_s} \xi_{i_s^-}^{(p_1 p_2)} \Xi_{\mathbf{k}_s^-}^{(r_1 r_2)} + \sqrt{(i_s + 1) k_s} \xi_{i_s^+}^{(p_1 p_2)} \Xi_{\mathbf{k}_s^-}^{(r_1 r_2)} + \sqrt{i_s (k_s + 1)} \xi_{i_s^-}^{(p_1 p_2)} \Xi_{\mathbf{k}_s^+}^{(r_1 r_2)} + \sqrt{(i_s + 1)(k_s + 1)} \xi_{i_s^+}^{(p_1 p_2)} \Xi_{\mathbf{k}_s^+}^{(r_1 r_2)} \right\}$$

and

$$C_{r_1 r_2, r_3 r_4}^{(\text{ff})}(t) = C_0(t) \sum_{i, \mathbf{k}} \sum_s^N \left\{ \sqrt{i_s k_s} \Xi_{i_s^-}^{(r_1 r_2)} \Xi_{\mathbf{k}_s^-}^{(r_3 r_4)} + \sqrt{(i_s + 1) k_s} \Xi_{i_s^+}^{(r_1 r_2)} \Xi_{\mathbf{k}_s^-}^{(r_3 r_4)} \right. \\ \left. + \sqrt{i_s (k_s + 1)} \Xi_{i_s^-}^{(r_1 r_2)} \Xi_{\mathbf{k}_s^+}^{(r_3 r_4)} + \sqrt{(i_s + 1)(k_s + 1)} \Xi_{i_s^+}^{(r_1 r_2)} \Xi_{\mathbf{k}_s^+}^{(r_3 r_4)} \right\},$$

where

$$\Xi_{i_s^\pm}^{(r_1 r_2)} = \sum_{\substack{m, n \\ m > n}}^N \Psi_{r_1, i}^{(mn)*} \Psi_{r_2, i_s^\pm}^{(mn)}. \quad (\text{A3})$$

Appendix B: Response functions for 2D photon echo spectra

We consider the photon-echo signals of the 2D electronic spectroscopy in the impulsive limit. In this limit, the laser pulses are assumed as infinitely short and, therefore, the measured intensity of electric field is proportional to the system response function, the expressions of which are presented in this appendix following the notation used in Fig. 2 [55]. The expressions for the response involve the spectral lineshape functions $g_{ab, cd}(t) \equiv h_{ab, cd} g_0(t)$. These are given by the linear integral transformation of the bath correlation functions, $g_0(t) = \int_0^t dt' \int_0^{t'} dt'' \langle C_0(t'') C_0(0) \rangle$ [44]. The response functions of the photon-echo (rephasing) signal when transport is ignored are then ($\mathbf{t} \equiv \{t_3, t_2, t_1\}$)

$$S_B(\mathbf{t}) = i^3 \theta(\mathbf{t}) \sum_{ij} \sum_{p_1 p_2} p_{g_i} (\delta_{i, j} G_{g_i g_i}(t_2) + \zeta_{i, j}) \quad (\text{B1}) \\ \times \left\langle \mu_{g_i}^{e_{p_1}} \mu_{e_{p_1}}^{g_j} \mu_{g_j}^{e_{p_2}} \mu_{e_{p_2}}^{g_i} \right\rangle e^{i \xi_{e_{p_1} g_i} t_1 - i \xi_{g_i g_j} t_2 - i \xi_{e_{p_2} g_j} t_3} \\ \times e^{\phi_{e_{p_1} g_j e_{p_2} g_i}(0, t_1, t_1 + t_2 + t_3, t_1 + t_2)},$$

$$S_E(\mathbf{t}) = i^3 \theta(\mathbf{t}) \sum_{ij} \sum_{p_1 p_2} p_{g_i} (\delta_{p_1 p_2} G_{e_{p_1} e_{p_2}}(t_2) + \zeta_{p_1 p_2}) \quad (\text{B2}) \\ \times \left\langle \mu_{g_i}^{e_{p_1}} \mu_{g_i}^{e_{p_2}} \mu_{e_{p_2}}^{g_j} \mu_{e_{p_2}}^{g_i} \right\rangle e^{i \xi_{e_{p_1} g_i} t_1 - i \xi_{e_{p_2} e_{p_1}} t_2 - i \xi_{e_{p_1} g_j} t_3} \\ \times e^{\phi_{e_{p_1} g_j e_{p_2} g_i}(0, t_1 + t_2, t_1 + t_2 + t_3, t_1)}$$

and

$$S_A(\mathbf{t}) = -i^3 \theta(\mathbf{t}) \sum_i \sum_{p_1 p_2} \sum_r p_{g_i} (\delta_{p_1 p_2} G_{e_{p_1} e_{p_1}}(t_2) + \zeta_{p_1 p_2}) \quad (\text{B3}) \\ \times \left\langle \mu_{g_i}^{e_{p_1}} \mu_{g_i}^{e_{p_2}} \mu_{e_{p_2}}^{f_r} \mu_{f_r}^{e_{p_1}} \right\rangle e^{i \xi_{e_{p_1} g_i} t_1 - i \xi_{e_{p_2} e_{p_1}} t_2 - i \xi_{f_r, e_{p_1}} t_3} \\ \times e^{\phi_{e_{p_1} f_r e_{p_2} g_i}(0, t_1 + t_2 + t_3, t_1 + t_2, t_1)}.$$

Here, the complex variable $\xi_{ab} = \omega_{ab} - i \frac{1}{2}(\gamma_a + \gamma_b)$ is used to take into account the state dephasing due to finite lifetime, $\gamma_a = \frac{1}{2} \sum_{a' \neq a} k_{a \leftarrow a'}$. p_{g_i} is the Boltzmann

probability for the system to be in the i -th vibrational state prior the excitation and $\theta(\mathbf{t})$ is the product of Heaviside functions, $\theta(t_1)\theta(t_2)\theta(t_3)$. The auxiliary function is

$$\phi_{e_{p_1} c e_{p_2} g_i}(\tau_4, \tau_3, \tau_2, \tau_1) = \\ -g_{e_{p_1} e_{p_1}}(\tau_{43}) - g_{cc}(\tau_{32}) - g_{e_{p_2} e_{p_2}}(\tau_{21}) \quad (\text{B4}) \\ + g_{e_{p_1} c}(\tau_{32}) + g_{e_{p_1} c}(\tau_{43}) - g_{e_{p_1} c}(\tau_{42}) \\ - g_{e_{p_1} e_{p_2}}(\tau_{32}) + g_{e_{p_1} e_{p_2}}(\tau_{31}) + g_{e_{p_1} e_{p_2}}(\tau_{42}) \\ - g_{e_{p_1} e_{p_2}}(\tau_{41}) + g_{c e_{p_2}}(\tau_{21}) + g_{c e_{p_2}}(\tau_{32}) - g_{c e_{p_2}}(\tau_{31}) \\ - g_{c g_i}(\tau_{21}) + g_{c g_i}(\tau_{24}) + g_{c g_i}(\tau_{31}) - g_{c g_i}(\tau_{34}),$$

where c stands for either doubly-excited state f_r , either ground state g_j . Response function components with transport are

$$\tilde{S}_B(\mathbf{t}) = i^3 \theta(\mathbf{t}) \sum_{ij} \sum_{p_1 p_2} p_{g_i} \zeta_{ij} G_{g_j g_i}(t_2) \quad (\text{B5}) \\ \times \left\langle \mu_{g_i}^{e_{p_1}} \mu_{e_{p_1}}^{g_i} \mu_{g_j}^{e_{p_2}} \mu_{e_{p_2}}^{g_j} \right\rangle e^{i \xi_{e_{p_1} g_i} t_1 - i \xi_{e_{p_2} g_j} t_3 + \varphi_{e_{p_2} g_j e_{p_2} e_{p_1}}^*(\mathbf{t})},$$

$$\tilde{S}_E(\mathbf{t}) = i^3 \theta(\mathbf{t}) \sum_{ij} \sum_{p_1 p_2} p_{g_i} \zeta_{p_1 p_2} G_{e_{p_2} e_{p_1}}(t_2) \quad (\text{B6}) \\ \times \left\langle \mu_{g_i}^{e_{p_1}} \mu_{g_i}^{e_{p_1}} \mu_{e_{p_2}}^{g_j} \mu_{e_{p_2}}^{g_j} \right\rangle e^{i \xi_{e_{p_1} g_i} t_1 - i \xi_{e_{p_2} g_j} t_3 + \varphi_{e_{p_2} g_j e_{p_2} e_{p_1}}^*(\mathbf{t})},$$

and

$$\tilde{S}_A(\mathbf{t}) = -i^3 \theta(\mathbf{t}) \sum_i \sum_{p_1 p_2} \sum_r p_{g_i} \zeta_{p_1 p_2} G_{e_{p_2} e_{p_1}}(t_2) \quad (\text{B7}) \\ \times \left\langle \mu_{g_i}^{e_{p_1}} \mu_{g_i}^{e_{p_1}} \mu_{e_{p_2}}^{f_r} \mu_{f_r}^{e_{p_2}} \right\rangle e^{i \xi_{e_{p_1} g_i} t_1 - i \xi_{f_r, e_{p_2}} t_3 + \varphi_{f_r, e_{p_2} e_{p_2} e_{p_1}}^*(\mathbf{t})}.$$

Here

$$\varphi_{c b e_{p_2} e_{p_1}}(\mathbf{t}) = -g_{e_{p_1} e_{p_1}}(t_1) - g_{bb}(t_3) - g_{cc}^*(t_3) \\ - g_{b e_{p_1}}(t_1 + t_2 + t_3) + g_{b e_{p_1}}(t_1 + t_2) + g_{b e_{p_1}}(t_2 + t_3) \\ - g_{b e_{p_1}}(t_2) + g_{c e_{p_1}}(t_1 + t_2 + t_3) - g_{c e_{p_1}}(t_1 + t_2) \\ - g_{c e_{p_1}}(t_2 + t_3) + g_{c e_{p_1}}(t_2) + g_{cb}(t_3) + g_{cb}^*(t_3) \\ + 2i \Im [g_{c e_{p_2}}(t_2 + t_3) - g_{c e_{p_2}}(t_2) - g_{c e_{p_2}}(t_3) \\ + g_{b e_{p_2}}(t_2) - g_{b e_{p_2}}(t_2 + t_3) + g_{b e_{p_2}}(t_3)]. \quad (\text{B8})$$

- [1] A. Davydov. *A Theory of Molecular Excitations*. Mc.Graw-Hill, New York, 1962.
- [2] E.I. Rashba, E.F. Sheka, and V.I. Broude. *Spectroscopy of Molecular Excitons*. Springer, Berlin, 1985.
- [3] A. Nemeth, F. Milota, T. Mančal, V. Lukeš, J. Hauer, H.F. Kauffmann, and J. Sperling. Vibrational wave packet induced oscillations in two-dimensional electronic spectra. I. Experiments. *J. Chem. Phys.*, 132:184514, 2010.
- [4] D. Egorova, M.F. Gelin, and W. Domcke. Analysis of vibrational coherences in homodyne and two-dimensional heterodyne photon-echo spectra of Nile Blue. *Chem. Phys.*, 341(1):113–122, 2007.
- [5] E.R. Smith and D.M. Jonas. Alignment, vibronic level splitting, and coherent coupling effects on the pump-probe polarization anisotropy. *J. Phys. Chem. A*, 115(16):4101–4113, 2011.
- [6] M. Dahlbom, W. Beenken, V. Sundström, and T. Pullerits. Collective excitation dynamics and polaron formation in molecular aggregates. *Chem. Phys. Lett.*, 364(5):556–561, 2002.
- [7] A. Gelzinis, D. Abramavicius, and L. Valkunas. Non-markovian effects in time-resolved fluorescence spectrum of molecular aggregates: Tracing polaron formation. *Phys. Rev. B*, 84:245430, 2011.
- [8] T.D. Huynh, K.-W. Sun, M. Gelin, and Y. Zhao. Polaron dynamics in two-dimensional photon-echo spectroscopy of molecular rings. *J. Chem. Phys.*, 139:104103, 2013.
- [9] A.W. Chin, J. Prior, R. Rosenbach, F. Caycedo-Soler, S.F. Huelga, and M.B. Plenio. The role of non-equilibrium vibrational structures in electronic coherence and recoherence in pigment-protein complexes. *Nature Phys.*, 9:113–118, 2013.
- [10] N. Christensson, H.F. Kauffmann, T. Pullerits, and T. Mančal. Origin of long-lived coherences in light-harvesting complexes. *J. Phys. Chem. B*, 116(25):7449–7454, 2012.
- [11] C. Kreisbeck and T. Kramer. Long-lived electronic coherence in dissipative exciton dynamics of light-harvesting complexes. *J. Phys. Chem. Lett.*, 3(19):2828–2833, 2012.
- [12] R.L. Fulton and M. Gouterman. Vibronic coupling. II. Spectra of dimers. *J. Chem. Phys.*, 41(8):2280–2286, 1964.
- [13] M.R. Philpott. Theory of the coupling of electronic and vibrational excitations in molecular crystals and helical polymers. *J. Chem. Phys.*, 55:2039, 1971.
- [14] A.S. Davydov and A.A. Serikov. Vibronic spectra of crystals at arbitrary shifts of the atomic equilibrium positions in the molecules. *Phys. Status Solidi B*, 42(2):603–615, 1970.
- [15] A.S. Davydov and A.A. Serikov. Vibronic spectra of molecular crystals under totally symmetric vibrations. *Phys. Status Solidi B*, 44(1):127–138, 1971.
- [16] R. Friesner and R. Silbey. Exciton-phonon coupling in a dimer: An analytic approximation for eigenvalues and eigenvectors. *J. Chem. Phys.*, 74:1166, 1981.
- [17] P.O.J. Scherer and S.F. Fischer. On the theory of vibronic structure of linear aggregates. application to pseudoisocyanin (PIC). *Chem. Phys.*, 86(3):269–283, 1984.
- [18] F. Milota, V.I. Prokhorenko, T. Mančal, H. von Berlepsch, O. Bixner, H.F. Kauffmann, and J. Hauer. Vibronic and vibrational coherences in two-dimensional electronic spectra of supramolecular J-aggregates. *J. Phys. Chem. A*, 117:6007–6014, 2013.
- [19] T. Kobayashi. *J – aggregates*. World Scientific, Singapore, 1996.
- [20] W. West and S. Pearce. The dimeric state of cyanine dyes. *J. Phys. Chem.*, 69(6):1894–1903, 1965.
- [21] B. Kopaínský, J.K. Hallermeier, and W. Kaiser. The first step of aggregation of PIC: The dimerization. *Chem. Phys. Lett.*, 83(3):498–502, 1981.
- [22] I. Baraldi, M. Caselli, F. Momicchioli, G. Ponterini, and D. Vanossi. Dimerization of green sensitizing cyanines in solution. A spectroscopic and theoretical study of the bonding nature. *Chem. Phys.*, 275(1):149–165, 2002.
- [23] A.M. Moran, J.B. Maddox, J.W. Hong, J. Kim, R.A. Nome, G.C. Bazan, S. Mukamel, and N.F. Scherer. Optical coherence and theoretical study of the excitation dynamics of a highly symmetric cyclophane-linked oligophenylenevinylene dimer. *J. Chem. Phys.*, 124:194904, 2006.
- [24] J. Seibt, V. Dehm, F. Würthner, and V. Engel. Circular dichroism spectroscopy of small molecular aggregates: Dynamical features and size effects. *J. Chem. Phys.*, 128:204303, 2008.
- [25] O. Bixner, V. Lukeš, T. Mančal, J. Hauer, F. Milota, M. Fischer, I. Pugliesi, M. Bradler, W. Schmid, E. Riedle, H.F. Kauffmann, and N. Christensson. Ultrafast photo-induced charge transfer unveiled by two-dimensional electronic spectroscopy. *J. Chem. Phys.*, 136:204503, 2012.
- [26] A. Kolli, E.J. O’Reilly, G.D. Scholes, and A. Olaya-Castro. The fundamental role of quantized vibrations in coherent light harvesting by cryptophyte algae. *J. Chem. Phys.*, 137(17):174109–174109, 2012.
- [27] J. Adolphs and T. Renger. How proteins trigger excitation energy transfer in the FMO complex of green sulfur bacteria. *Biophys. J.*, 91:2778–2797, 2006.
- [28] H. Lee, Y.-C. Cheng, and G.R. Fleming. Coherence dynamics in photosynthesis: Protein protection of excitonic coherence. *Science*, 316:1462–1465, 2007.
- [29] J.M. Womick and A.M. Moran. Vibronic enhancement of exciton sizes and energy transport in photosynthetic complexes. *J. Phys. Chem. B*, 115(6):1347–1356, 2011.
- [30] G.H. Richards, K.E. Wilk, P.M.G. Curmi, H.M. Quiney, and J.A. Davis. Coherent vibronic coupling in light-harvesting complexes from photosynthetic marine algae. *J. Phys. Chem. Lett.*, 3(2):272–277, 2012.
- [31] G.S. Engel, T.R. Calhoun, E.L. Read, T.K. Ahn, T. Mančal, Y.-C. Cheng, R.E. Blankenship, and G.R. Fleming. Evidence for wavelike energy transfer through quantum coherence in photosynthetic systems. *Nature*, 446:782, 2007.
- [32] E. Collini, C.Y. Wong, K.E. Wilk, P.M.G. Curmi, P. Brumer, and G.D. Scholes. Coherently wired light-harvesting in photosynthetic marine algae at ambient temperature. *Nature*, 463:644–647, 2010.
- [33] G. Panitchayangkoon, D.V. Voronine, D. Abramavicius, J.R. Caram, N.H.C. Lewis, S. Mukamel, and G.S. Engel. Direct evidence of quantum transport in photosynthetic light-harvesting complexes. *Proc. Natl. Acad. Sci. USA*, 108(52):20908–20912, 2011.
- [34] N. Christensson, F. Milota, J. Hauer, J. Sperling,

- O. Bixner, A. Nemeth, and H.F. Kauffmann. High frequency vibrational modulations in two-dimensional electronic spectra and their resemblance to electronic coherence signatures. *J. Phys. Chem. B*, 115(18):5383–5391, 2011.
- [35] V. Tiwari, W.K. Peters, and D.M. Jonas. Electronic resonance with anticorrelated pigment vibrations drives photosynthetic energy transfer outside the adiabatic framework. *Proc. Natl. Acad. Sci. USA*, 110(4):1203–1208, 2013.
- [36] Q. Liu, J. Ye, and Y. Zhao. Multimode vibronic spectra of the Holstein molecular crystal model. *Phys. Chem. Chem. Phys.*, 12(23):6045–6053, 2010.
- [37] A. Halpin, P.J.M. Johnson, R.S. Murphy, V.I. Prokhorenko, and R.J.D. Miller. Two-dimensional electronic spectroscopy of a model dimer system. *EPJ Web of Conferences*, 41:05032, 2013.
- [38] F.C. Spano, J. Clark, C. Silva, and R.H. Friend. Determining exciton coherence from the photoluminescence spectral line shape in poly (3-hexylthiophene) thin films. *J. Chem. Phys.*, 130:074904, 2009.
- [39] H. Fidler. Absorption and emission studies on pure and mixed J-aggregates of pseudoisocyanine. *Chem. Phys.*, 341:158–168, 2007.
- [40] T. Holstein. Studies of polaron motion: Part I. The molecular-crystal model. *Ann. Phys.*, 8(3):325–342, 1959.
- [41] S. Polyutov, O. Kühn, and T. Pullerits. Exciton-vibrational coupling in molecular aggregates: Electronic versus vibronic dimer. *Chem. Phys.*, 394(1):21–28, 2012.
- [42] A. Chenu, N. Christensson, H.F. Kauffmann, and T. Mančal. Enhancement of vibronic and ground-state vibrational coherences in 2D spectra of photosynthetic complexes. *Sci. Rep.*, 3:2029, 2013.
- [43] V. Butkus, D. Zigmantas, D. Abramavicius, and L. Valkunas. Distinctive character of electronic and vibrational coherences in disordered molecular aggregates. *Chem. Phys. Lett. ASAP*, 2013.
- [44] S. Mukamel. *Principles of Nonlinear Optical Spectroscopy*. Oxford University Press, New York, 1995.
- [45] V. May and O. Kühn. *Charge and Energy Transfer Dynamics in Molecular Systems*. Wiley-VCH, Weinheim, 2011.
- [46] L. Valkunas, D. Abramavicius, and T. Mančal. *Molecular Excitation Dynamics and Relaxation*. Wiley-VCH, Weinheim, 2013.
- [47] T. Mančal, A. Nemeth, F. Milota, V. Lukeš, H.F. Kauffmann, and J. Sperling. Vibrational wave packet induced oscillations in two-dimensional electronic spectra. II. Theory. *J. Chem. Phys.*, 132:184515, 2010.
- [48] D. Egorova. Detection of electronic and vibrational coherences in molecular systems by 2D electronic photon echo spectroscopy. *Chem. Phys.*, 347(1-3):166–176, 2008.
- [49] V. Butkus, L. Valkunas, and D. Abramavicius. Molecular vibrations-induced quantum beats in two-dimensional electronic spectroscopy. *J. Chem. Phys.*, 137(4):044513, 2012.
- [50] J. Seibt, T. Hansen, and T. Pullerits. 3D spectroscopy of vibrational coherences in quantum dots: Theory. *J. Phys. Chem. B*, 117:11124–11133, 2013.
- [51] J. Krčmář, M.F. Gelin, and W. Domcke. Calculation of third-order signals via driven Schrödinger equations: General results and application to electronic 2D photon echo spectroscopy. *Chem. Phys.*, 422:53–62, 2013.
- [52] H. van Amerongen, L. Valkunas, and R. van Grondelle. *Photosynthetic Excitons*. World Scientific Co., Singapore, 2000.
- [53] F.C. Spano. The spectral signatures of Frenkel polarons in H- and J-aggregates. *Acc. Chem. Res.*, 43(3):429–439, 2009.
- [54] A. Eisfeld, L. Braun, W.T. Strunz, J.S. Briggs, J. Beck, and V. Engel. Vibronic energies and spectra of molecular dimers. *J. Chem. Phys.*, 122(13):134103, 2005.
- [55] D. Abramavicius, B. Palmieri, D.V. Voronine, F. Šanda, and S. Mukamel. Coherent multidimensional optical spectroscopy of excitons in molecular aggregates; Quasiparticle versus supermolecule perspectives. *Chem. Rev.*, 109:2350–2408, 2009.
- [56] J. Seibt, P. Marquetand, V. Engel, Z. Chen, V. Dehm, and F. Würthner. On the geometry dependence of molecular dimer spectra with an application to aggregates of perylene bisimide. *Chem. Phys.*, 328(1):354–362, 2006.
- [57] V. Butkus, D. Zigmantas, L. Valkunas, and D. Abramavicius. Vibrational vs. electronic coherences in 2D spectrum of molecular systems. *Chem. Phys. Lett.*, 545:40–43, 2012.
- [58] N. Christensson, K. Židek, N.C.M. Magdaong, A.M. LaFountain, H.A. Frank, and D. Zigmantas. Origin of the bathochromic shift of astaxanthin in lobster protein: 2D electronic spectroscopy investigation of β -crustacyanin. *J. Phys. Chem. B*, 117(38):11209–11219, 2013.
- [59] T.R. Calhoun, N.S. Ginsberg, G.S. Schlau-Cohen, Y.-C. Cheng, M. Ballottari, R. Bassi, and G.R. Fleming. Quantum coherence enabled determination of the energy landscape in light-harvesting complex II. *J. Phys. Chem. B*, 113:16291–16295, 2009.
- [60] D.B. Turner, R. Dinshaw, K.-K. Lee, M. Belsley, K.E. Wilk, P.M.G. Curmi, and G.D. Scholes. Quantitative investigations of quantum coherence for a light-harvesting protein at conditions simulating photosynthesis. *Phys. Chem. Chem. Phys.*, 14:4857–4874, 2012.
- [61] A. Kell, X. Feng, M. Reppert, and R.J. Jankowiak. On the shape of the phonon spectral density in photosynthetic complexes. *J. Phys. Chem. B*, 117:7317–7323, 2013.